Reporting neural activity with genetically encoded calcium indicators

S. Andrew Hires, Lin Tian and Loren L. Looger*
Howard Hughes Medical Institute, Janelia Farm Research Campus, 19700 Helix Dr, Ashburn,
VA 20147, USA (*author for correspondence; e-mail: loogerl@janelia.hhmi.org)

Genetically encoded calcium indicators (GECIs), based on recombinant fluorescent proteins, have been engineered to observe calcium transients in living cells and organisms. Through observation of calcium, these indicators also report neural activity. We review progress in GECI construction and application, particularly toward *in vivo* monitoring of sparse action potentials (APs). We summarize the extrinsic and intrinsic factors that influence GECI performance. A simple model of GECI response to AP firing demonstrates the relative significance of these factors. We recommend a standardized protocol for evaluating GECIs in a physiologically relevant context. A potential method of simultaneous optical control and recording of neuronal circuits is presented.

Introduction

The intracellular concentration of free divalent calcium ions, $[Ca^{2+}]$, is a ubiquitous second messenger that regulates a wide range of cellular functions (Burgoyne, 2007). The magnitude of physiological changes in $[Ca^{2+}]$ is uniquely high among all intracellular ions (Hille, 1992). In neurons, action potential (AP) firing triggers large influxes of Ca^{2+} through voltage-gated calcium channels located throughout the cell (Jaffe et al., 1992). Synaptic input causes local Ca^{2+} influx through neurotransmitter receptors in dendritic spines and shaft (Muller and Connor, 1991). The spatiotemporal pattern of intracellular $[Ca^{2+}]$ is tightly coupled to neural activity (Denk et al., 1996). Therefore, the timing of spikes and patterns of synaptic input can be monitored by observing intracellular $[Ca^{2+}]$ (Yasuda et al., 2004; Denk et al., 1996; Yuste and Denk, 1995; Yuste et al., 1999).

Historically, intracellular calcium has been monitored by impaling cells on calcium-sensitive microelectrodes (Rink et al., 1980), by microinjection of bioluminescent proteins (Johnson and Shimomura, 1972), and with synthetic non-fluorescent metallochromic dyes (Tsien and Rink, 1983). The modern era of calcium imaging began with the synthesis of fluorescent dyes based on BAPTA, the highly selective calcium chelator (Tsien, 1980). These include fura (Grynkiewicz et al., 1985), quin (Tsien, 1980), indo (Grynkiewicz et al., 1985), fluo (Minta et al., 1989), and rhod (Minta et al., 1989) dyes. Commercial labs have further diversified these probes (Haugland et al., 2005). Each modern dye has a subset of desirable properties: Ca^{2+}-dependent fluorescence increase of >100-fold, high specificity for Ca^{2+} over other divalent cations, tuned affinity by chlorination or fluorination, fast kinetics, varied excitation and emission spectra, fluorescent intensity or wavelength ratiometric readout, and defined cell permeability (Tsien, 1999). These dyes can reliably quantify the changes in intracellular calcium associated with neural activity (Yasuda et al., 2004). However,

these small molecule probes have limitations: they can be difficult to introduce into neurons in the intact brain (Kerr and Denk, 2008), they can accumulate in high-$[Ca^{2+}]$ intracellular compartments (Di Virgilio et al., 1988), and many are extruded from the cytoplasm in several hours (Di Virgilio et al., 1988). Furthermore, chronic repeated measurements from the same cells *in vivo* are impossible, and the dyes cannot be targeted to specific cell types, populations, or subcellular locations without added transgenes (Tour et al., 2007).

Genetically encoded calcium indicators (GECIs) based on recombinant fluorescent proteins (FPs) address many of the shortcomings of small molecule dyes. GECIs can be delivered in a minimally invasive manner to specific cell types or subcellular compartments (Miyawaki et al., 1997). They are compatible with long-term, repeated, *in vivo* measurements (Hasan et al., 2004). GECIs have successfully recorded *in vivo* neural activity in brain regions with large modulation of dense spiking (Kerr et al., 2000; Fiala et al., 2002; Hasan et al., 2004), though recording of sparse spike trains remains elusive (Mank and Griesbeck, 2008). Through iterative cycles of optimization, GECIs are now able to occasionally detect single APs, at least under ideal *ex vivo* imaging conditions (Mao et al., 2008). Once single-AP detection can be consistently achieved *in vivo*, GECIs will revolutionize analysis of neural circuit dynamics. However, at their current state of development, GECIs still have significant drawbacks. The best GECIs remain inferior to synthetic dyes in signal-to-noise (SNR), kinetics, linearity, photostability, and ion selectivity (Mank and Griesbeck, 2008; Tsien, 1999). Of additional concern *in vivo*, GECIs can bind and interfere with endogenous signaling molecules (Hasan et al., 2004; Palmer and Tsien, 2006), and protein stability and fluorescence properties often suffer at physiological temperatures (Nakai et al., 2001).

Since proper application of GECIs requires a significant investment in time and resources, selection of the most appropriate GECI at the start of a project is paramount. Previous reviews have outlined strategies for GECI construction (Miyawaki and Tsien, 2000; Mank and Griesbeck, 2008), optimization (Shimozono and Miyawaki, 2008), and expression (Kotlikoff, 2007). Detailed protocols for quantitative calcium measurement with GECIs are available (Palmer and Tsien, 2006; Kerr and Schafer, 2006; Truong et al., 2007). Comparisons of GECI performance have been made in mouse brain slice (Pologruto et al., 2004; Mao et al., 2008), *Drosophila* larval neuromuscular junction (Reiff et al., 2005; Mank et al., 2006), and intact mouse brain (Hasan et al., 2004). In this paper, we analyze factors that affect GECI performance, specifically for detection of neural activity, and predict how future optimization will improve this performance. This information can guide GECI selection.

GECI construction strategies

A GECI comprises a calcium-binding recognition element allosterically coupled to an optical reporter element. Most GECI recognition elements are based on naturally evolved calcium-binding proteins with large Ca^{2+}-dependent conformational changes such as calmodulin (CaM) (Miyawaki et al., 1997; Nakai et al., 2001) or troponin-C (TnC) (Heim and Griesbeck, 2004). Wild-type recognition elements have been engineered to improve binding and response properties (Palmer et al., 2006; Garaschuk et al., 2007). Many GECIs use a conformational actuator to magnify the Ca^{2+}-dependent conformational change. The classical example is the M13 peptide (M13pep) from myosin light chain kinase, which preferentially binds to the calcium-bound form of calmodulin (Miyawaki et al., 1997).

There are two classes of GECI reporter elements: single fluorescent proteins (FPs) or Fluorescence Resonance Energy Transfer (FRET) donor–acceptor FP pairs. Single-FP reporter elements typically comprise a circularly permuted or split FP whose fluorescence properties (emission wavelength or intensity) are modulated by recognition element-dependent changes in chromophore protonation state or strain (Baird et al., 1999; Nagai et al., 2001; Nakai et al., 2001). In 2-FP GECIs, conformational changes in the recognition element modulate FRET transfer efficiency between the FP pair, altering the emission intensity of both donor and acceptor (Miyawaki et al., 1997; Heim and Griesbeck, 2004). The molecular architecture of several representative GECIs is shown in Fig. 1.
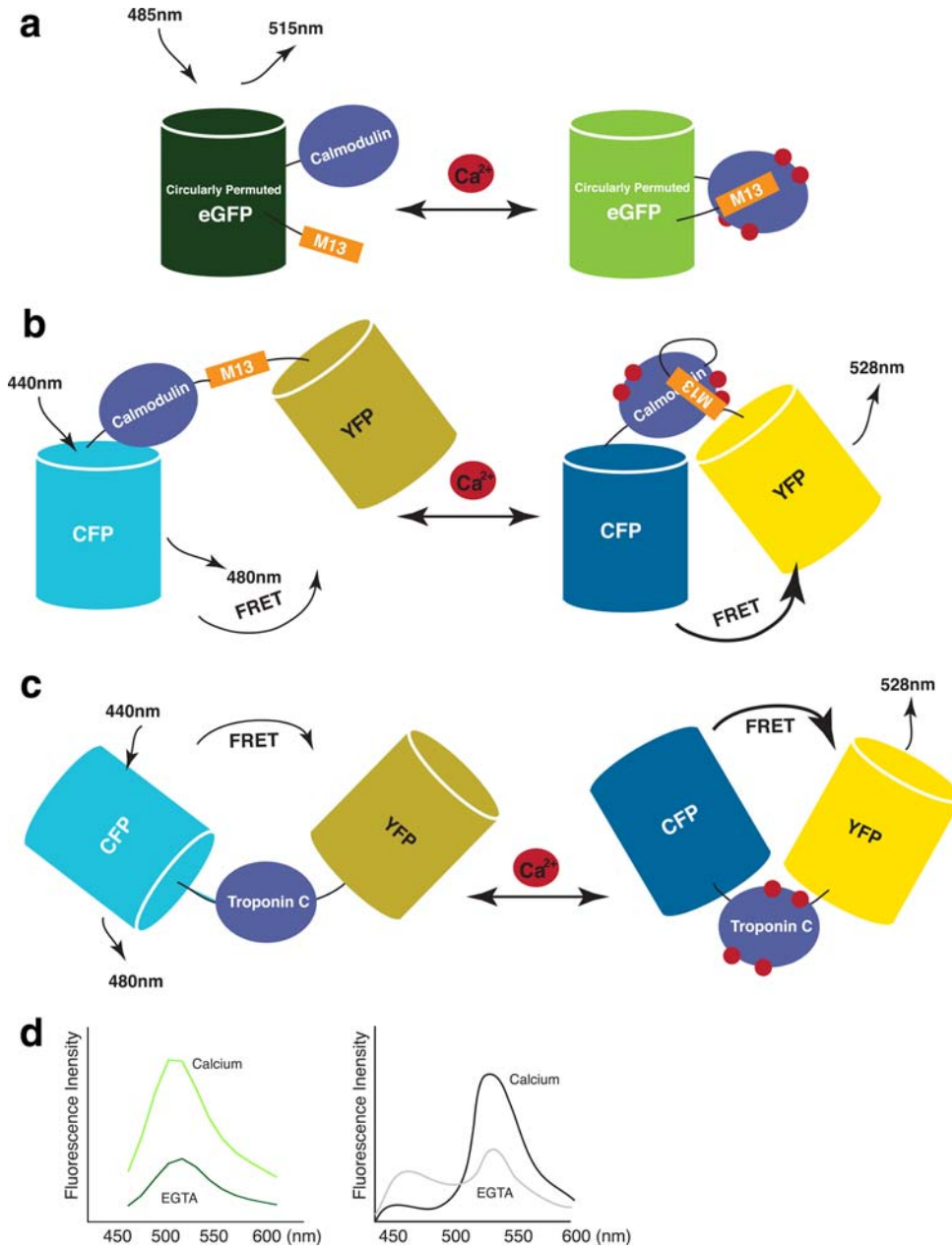
Fig. 1. Schematic representation of several commonly used genetically encoded Ca^{2+} indicators (GECIs). GECIs are based either on change of florescence of a single fluorophore (a) or change in fluorescence resonance energy transfer (FRET) efficiency (b, c). (a) Schematic of G-CaMP sensing mechanism. Upon calcium binding, conformational change of CaM and formation of the CaM-M13pep complex increases the fluorescence of the circularly permuted GFP. (b) The cameleon family of FRET-based GECIs, in which CaM and the M13 peptide are bracketed by a FRET pair. Calcium binding to calmodulin increases emission from the FRET acceptor. (c) Troponin-based FRET GECIs, in which the skeletal muscle calcium sensor troponin-C (TnC) is bracketed by a FRET pair. Binding of calcium to TnC leads to a conformational change and an increase in FRET acceptor emission. (d) Schematic representations of the fluorescence change for G-CaMPs (*left*) and FRET indicators (*right*). In (b) and (c), CFP and YFP represent generic FRET donors and acceptors. These may be engineered or circularly permuted versions of eCFP and eYFP, or they may be alternate fluorescent proteins.

Performance of current GECIs

The challenge of using GECIs for functional neuronal imaging can be illustrated by comparing the performance of a state-of-the-art GECI, G-CaMP2, to that of a simultaneously recorded intracellular synthetic dye, X-Rhod-5F (Fig. 2a). In response to high-frequency trains of APs (40AP at 83 Hz), G-CaMP2's change in fluorescence over baseline ($\Delta F/F_0$) slightly exceeds that of X-Rhod-5F. However, during briefer trains, the GECI response is relatively small. A single AP can be reliably detected with the synthetic indicator but not with the GECI (Fig. 2a) (Mao et al., 2008). The SNR of the measurement is defined by the ratio of the signal change ($\Delta F = F_{obs} - F_0$; where F_{obs} is sensor fluorescence at peak [Ca^{2+}], F_0 is sensor fluorescence at baseline [Ca^{2+}]) to the shot noise of baseline fluorescence ($\sim F_0 N^{-1/2}$) such that

$$SNR = \frac{\Delta F}{F_0} N^{1/2} \tag{1}$$

where N is the number of photons detected (Yasuda et al., 2004). The dye has a noise level approximately 10-fold lower than the GECI. Although X-Rhod-5F is much dimmer than GFP (rhod-2's $EC \times QE \approx 8,300$ at saturating calcium vs. 33,000 for EGFP), it has a relatively low affinity, one binding site, does not bind endogenous proteins and is acutely introduced. Therefore, it can be used at much higher concentrations than G-CaMP2, reducing noise. There is also a large degree of cell-to-cell variability in GECI response magnitude and apparent kinetics (Figs. 2b and 3a) (Mao et al., 2008), which could cause considerable detection bias when imaging networks of interacting neurons. The basis of this variability remains under investigation.

Extrinsic properties that influence the performance of GECIs

Ca²⁺ dynamics

An *in vivo* AP lasts approximately 1 ms, with a rapid influx of Ca^{2+} occurring during the repolarization of the neuron back to baseline (Llinas et al., 1982). Calcium is actively extruded over a significantly longer period (Markram and Sakmann, 1994). The precise time course is dependent on

subcellular location, accessible volume, extrusion machinery, temperature, and the buffering capacity of the cytosol (and calcium indicator, if present). A broad time course allows more complete calcium binding to GECIs, increasing ΔF. Photons can be collected over a longer period than the underlying voltage spike, increasing N. It also lowers the sampling rate necessary to accurately capture the transient time course (Kerr and Denk, 2008). This allows simultaneous recording of spatially segregated calcium signals with single point excitation, as in two-photon laser scanning microscopy (2PLSM).

Action potentials occur at a wide range of frequencies. When sparse, each calcium transient is independent. When closely spaced, the calcium transients sum (Helmchen et al., 1996). Since the SNR of a GECI is generally insufficient to resolve a single AP (Mao et al., 2008), summation of closely spaced APs is necessary for GECI-based detection of neuronal spiking. Threshold effects make the interpretation of the absence of response problematic. For imaging data to be meaningful, the relationship between AP frequency and fluorescence response must be calibrated by simultaneous electrophysiology (Jayaraman and Laurent, 2007).

For a single AP, the change in free intracellular calcium $\Delta[Ca^{2+}]_i(t)$ can be expressed as a function of the resting calcium level $[Ca^{2+}]_0$, the total amount of calcium current injected by the AP $\Delta[Ca^{2+}]_T$, the calcium extrusion rate (γ) and the buffering capacity of the endogenous buffers (κ_S) and the GECI (κ_B). Buffering capacity is defined as $\Delta[Ca^{2+}]_T/\Delta[Ca^{2+}]_i$ and has been empirically determined in many cell types (Neher, 1995). The differential equations governing AP-mediated calcium transients have been explicitly solved (Neher, 1995; Helmchen et al., 1996). Prior to an AP ($t < 0$), $\Delta[Ca^{2+}]_i = 0$ and $[Ca^{2+}]_i = [Ca^{2+}]_0$. Immediately following an AP the calcium level spikes and subsequently decays such that:

$$\Delta[Ca^{2+}]_i = A \cdot e^{-t/\tau} \tag{2}$$

$$\tau = \frac{1 + \kappa_S + \kappa_B}{\gamma} \tag{3}$$

$$A = \frac{\Delta[Ca^{2+}]_T}{1 + \kappa_S + \kappa_B} \tag{4}$$

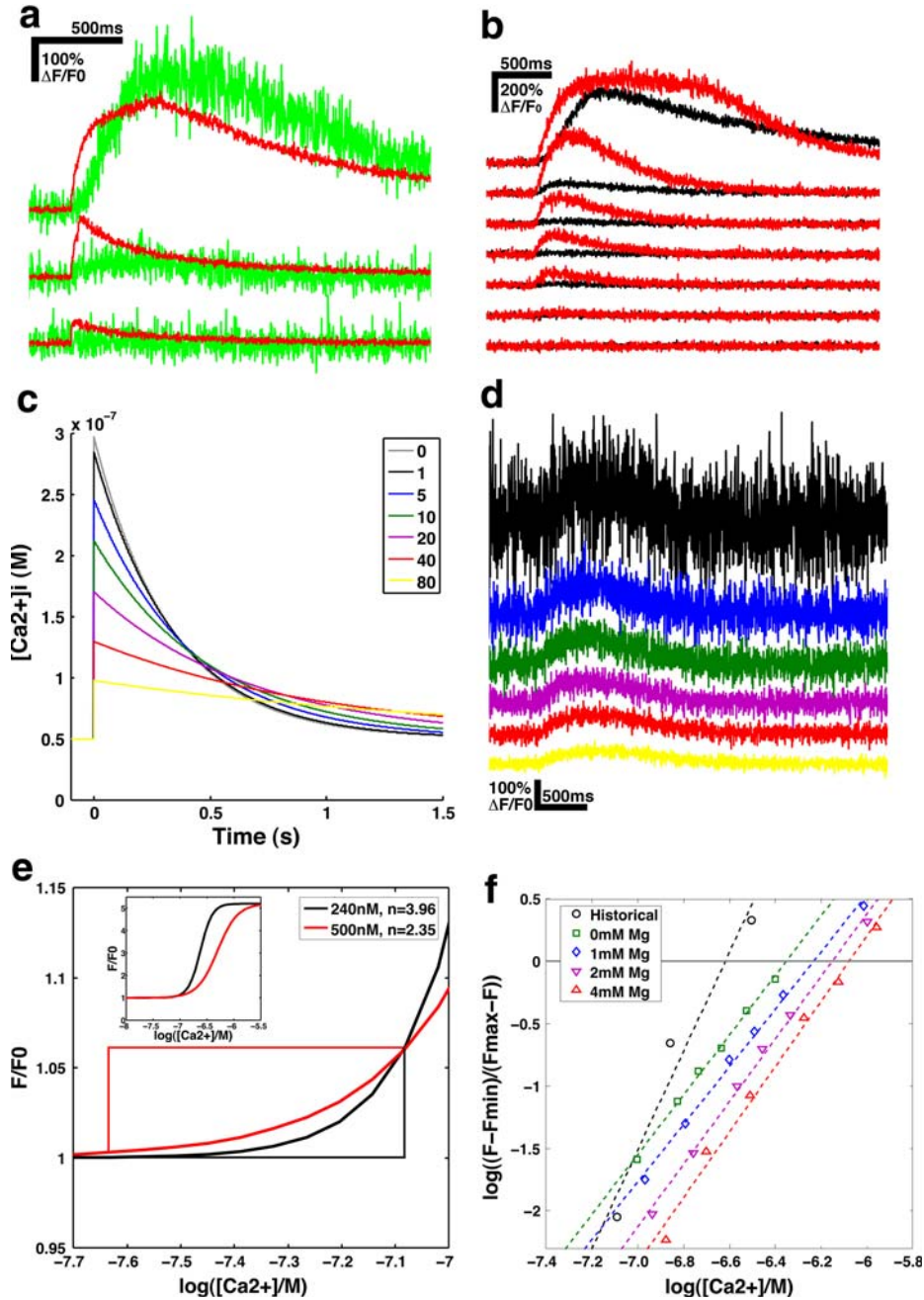In the case of a typical Layer V cortical pyramidal neuron measured near the base of the

Fig. 2. Properties that shape GECI response. (a) Typical fluorescence response of a G-CaMP2-expressing cell loaded with 500 μM X-Rhod-5F. Trains of 1, 5, and 40 AP delivered at 83 Hz by a whole-cell patch pipette. G-CaMP2 response in *green*, X-Rhod-5F response in *red*. (b) Variation of G-CaMP2 response to trains of 1, 2, 3, 4, 5, 10, and 40 APs, between two cells (*red*) and (*black*) of similar brightness, whole-cell parameters, and apparent health. (c) Increasing model [GECI] between 0, 1, 5, 10, 20, 40, 80 μM lowers the peak $\Delta[Ca^{2+}]_i$ transient and lengthens its time course. Model temperature is 22°C; $\tau \approx 330$ ms for the 0 μM case. (d) Increasing [GECI] improves the model's SNR at 10 AP despite lowering peak $\Delta[Ca^{2+}]_i$. Colors as in c. (e) Sensitivity of F_0 to the range of $[Ca^{2+}]_0$ in healthy neurons (23–83 nM). Affinity estimates derived from *in vitro* titrations of G-CaMP2 in historical buffer (*black*) or mock internal solution with 0.5 mM free Mg^{2+} (*red*). Inset shows titration over larger $[Ca^{2+}]$ range. (f) Titrations of G-CaMP2 in historical buffer or in mock internal solution with 0–4 mM Mg^{2+}.
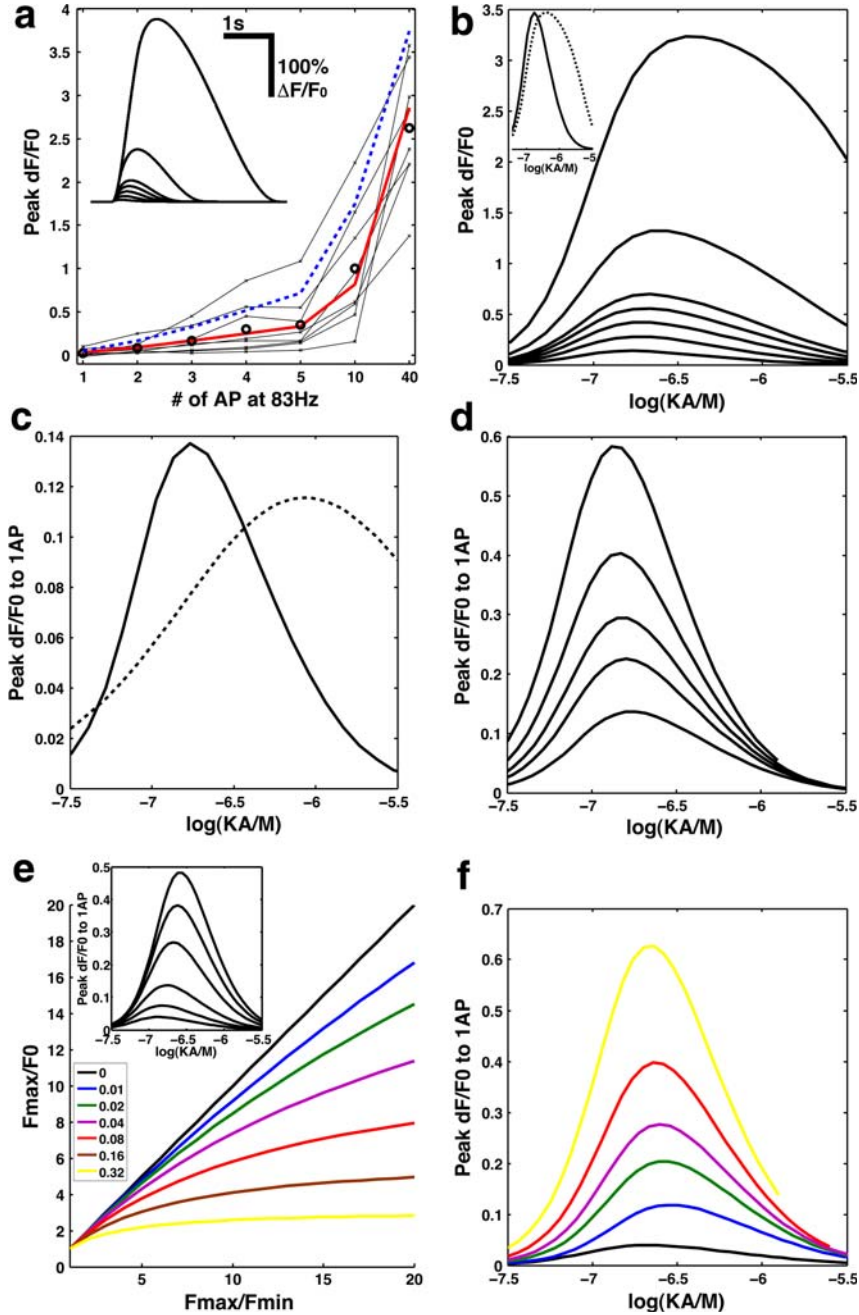
Fig. 3. (a) Comparison of GECI model's peak $\Delta F/F_0$ (*red line*) for 1, 2, 3, 4, 5, 10, and 40AP trains to individual G-CaMP2 responses (*thin lines*) and the mean G-CaMP2 response (*black circles*). Increasing model k_{on} and k_{off} 5-fold (*blue dotted line*) increases response. (a, inset) Model fluorescence time course. (b) Predicted peak change in fluorescence over baseline to AP trains (1, 2, 3, 4, 5, 10, 40) for a range of K_A values. (b, inset) 1AP (*solid*) and 40AP (*dotted*) trains normalized to optimal response. (c) Optimal affinity for 1AP response shifts between $n = 2.5$ (*solid*) and $n = 1$ (*dotted*). (d) Model response to 1AP increases with kinetic rates $k_{on} = (0.8, 1.6, 2.4, 4,$ and $8) \times 10^6$. (e) The dependence of effective dynamic range on total dynamic range is reduced as fractional saturation of model GECI at $[Ca^{2+}]_0$ increases from 0 to 0.32. (e, inset) Increasing total dynamic range ($F_{max}/F_{min} = 2, 3, 5, 10, 15, 20$) shifts the optimal K_A for single AP detection from 130 to 260 nM. (f) Responses to 1AP when time course of calcium transient decay is decreased to 70 ms. $n = 2.5$, $k_{on} = 8 \times 10^5$ M^{-1} s^{-1}, $F_{max}/F_{min} = 5$ (*black*), $k_{on} = (8, 16, 32, 40,$ and $80) \times 10^5$ M^{-1} s^{-1}, $F_{max}/F_{min} = 15$ (*colors*).

apical dendrite, $\kappa_S \approx 125$ and baseline $[Ca^{2+}]_0 \approx 50$ nM. In the absence of a perturbing indicator, peak $\Delta[Ca^{2+}]_i \approx 250$ nM and $\tau \approx 70$ ms per AP at 37°C (Helmchen et al., 1996). During brief trains, calcium fluxes from APs sum linearly (Helmchen et al., 1996). At room temperature, τ increases ~5-fold, due to slowed calcium extrusion, while peak $\Delta[Ca^{2+}]_i$ increases only slightly (Markram et al., 1995).

Intrinsic properties that influence the performance of GECIs

GECI expression levels
Fluorescence response of a GECI requires Ca^{2+} binding by the recognition element, thus GECIs inherently perturb calcium dynamics. Excessive [GECI] will significantly buffer AP-evoked calcium transients. Expression of high affinity cameleons in *Caenorhabditis elegans* buffers sufficient calcium (Suzuki et al., 2003) to affect behavior (Kindt et al., 2007) and rescues calcium-binding protein knockout phenotypes (Ferkey et al., 2007). To minimize GECI effects on the transient, κ_B should be significantly less than κ_S. However, raising [GECI] also improves SNR proportional to $[GECI]^{1/2}$ by increasing the number of photons collected, see Eq. 1 (Yasuda et al., 2004). The optimal [GECI] for an experiment strikes a balance between SNR and buffering.

The buffering capacity of an exogenous buffer is defined by its affinity, concentration, and resting intracellular $[Ca^{2+}]_0$ (Neher, 1995) such that

$$\kappa_B = \sum_{Ca^{2+} sites} \frac{[Ca^{2+} site] \cdot K_{d,i}}{\left(K_{d,i} + [Ca^{2+}]_0\right)^2} \qquad (5)$$

where $K_{d,i}$ is the dissociation constant (K_d) of each Ca^{2+}-binding site. For a hypothetical GECI with four equivalent sites of $K_d = 1$ μM at $[Ca^{2+}]_0 = 50$ nM, $\kappa_B \approx 1.32 \times 10^7$ $M^{-1} \cdot$ [GECI]. Increasing [GECI] will spread the free calcium over a longer-time period and lower the peak of the observed transient (Fig. 2c). The effect of [GECI] on SNR is illustrated by the hypothetical output of a model GECI to a 10 AP train at different [GECI] (Fig. 2d).

Assessment of the proper GECI expression level requires quantitative estimates of the relative expression of GECI to endogenous buffering capacity. This is most easily done by comparing fluorescence of purified GECI to intracellularly expressed GECI under identical imaging conditions (Tour et al., 2007). For FRET reporters, the emission of directly excited acceptor chromophore is used, as this is insensitive to calcium levels (Miyawaki and Tsien, 2000). For ratiometric single-FP sensors, the fluorescence isoemission wavelength, the point where emission intensity is insensitive to calcium, can be used. For intensity-modulated single-FP sensors, $[Ca^{2+}]_i$ must be independently measured or approximated, and corrected for. Resting calcium in healthy cortical pyramidal neurons at room temperature is approximately 53 ± 30 nM (Schiller et al., 1995). Using two different *in vitro* estimates of G-CaMP2 affinity and these $[Ca^{2+}]_0$ values, $F_0 \approx F_{min}$. The variation in [GECI] estimate due to variation in $[Ca^{2+}]_0$ is limited to ~5% (Fig. 2e).

In cultured HeLa cells, concentrations of YC3.1 below 20 μM were too dim for single cell imaging (Miyawaki et al., 1999). More sensitive GECIs, G-CaMP2 and YC3.60, have been used with epifluorescence illumination at 1.6 μM in mouse heart cytosol (Kotlikoff, 2007) and 1 μM in plant guard cells (Yang et al., 2008), respectively. In our study, using 2PLSM of acute cortical slices, [G-CaMP2] in recorded cells was 9.3 μM (std. dev. = 3.7 μM). Cells with [G-CaMP2] below 5 μM required unacceptably high laser intensity. Cells with [G-CaMP2] above 20 μM had attenuated responses for low AP bursts.

Misfolded or non-fluorescent GECIs may contribute to additional calcium buffering. A stoichiometric standard insensitive to calcium, such as a linear fusion to a reference FP, could be used to confirm [GECI], provided the standard did not perturb the function of the reporter. Alternative strategies include simultaneous translation of a reference FP using IRES (Pelletier and Sonenberg, 1988) or 2A peptide (Furler et al., 2001), and quantitative immunostaining.

Interference with endogenous Ca^{2+} signaling
In addition to buffering Ca^{2+}, GECI components (e.g., CaM, M13pep) may be sequestered by host proteins, resulting in higher fluorescence background and possible interference with development and signaling. Early attempts to target yellow cameleons to the plasma membrane resulted in non-functional indicators (Heim and Griesbeck, 2004), while generation of transgenic mice expressing yellow cameleons (YC3.0 and YC3.12,

respectively) under a constitutive (Tsai et al., 2003) and tetracycline-inducible promoter (Hasan et al., 2004) failed to show functional responses *in vivo*. Camgaroo2 and inverse pericam showed very modest responses when expressed under the inducible promoter system (Hasan et al., 2004). Fluorescence-recovery-after-photobleaching experiments indicated that half of the expressed inverse pericam was immobile (Hasan et al., 2004). These failures were attributed to interference, and inspired efforts to engineer probes orthogonal to endogenous calcium signaling molecules.

One approach to avoid endogenous interference was to substitute troponin-C, a skeletal calcium sensor not normally expressed in neurons, for calmodulin (Heim and Griesbeck, 2004). These GECI derivatives showed functional responses *in vivo* and form the basis of a major GECI class (e.g., TN-L15, TN-XL, TN-XXL) (Garaschuk et al., 2007; Mank and Griesbeck, 2008). Another strategy was the reengineering of the CaM-M13pep interface of yellow cameleons to favor intra- over inter-molecular interactions. These sensors (D1, D2cpv, D3cpv, and D4cpv) functioned when targeted to the plasma membrane and reliably reported calcium transients from single field stimulations in cultured hippocampal neurons (Palmer et al., 2006). In addition to increasing the proportion of functional GECI, the removal of interference may allow much higher levels of GECI expression *in vivo*, improving SNR.

GECI affinity

The sensitivity of a GECI is critically dependent on sensor affinity, kinetics and dynamic range, which influence responses to calcium transients in an interdependent way. Quantitative measurement of $[Ca^{2+}]$ is impossible without reliable estimates of all three parameters. The reported affinity of a single GECI can vary as much as 8-fold between *in vitro* and *in situ* titrations (Nakai et al., 2001; Pologruto et al., 2004). Discrepancies are likely due to differences in the biochemical milieu of the assay (Pologruto et al., 2004). Ionic strength can dramatically affect the maximum ratio change of FRET reporters (Hires et al., 2008) or the apparent affinity of the ligand-binding domain. Calmodulin's calcium affinity is reduced ~3-fold when assayed in 150 mM vs. 100 mM [KCl] (Linse et al., 1991), and both affinity and apparent cooperativity are reduced with increasing $[Mg^{2+}]$ (Ogawa and Tanokura, 1984).

Pipette internal solutions typically have ionic strength of ~0.17, yet nearly all published *in vitro* measurements on GECIs, including yellow cameleons (Miyawaki et al., 1997, 1999), reengineered cameleons (Palmer et al., 2006), pericams (Nagai et al., 2001), camgaroos (Baird et al., 1999), troponin-C based indicators (Mank et al., 2006), and G-CaMPs (Nakai et al., 2001; Ohkura et al., 2005) have been made in buffers with only 0.085–0.135 ionic strength (50–100 mM KCl or NaCl). Internal free $[Mg^{2+}]$ ranges from 0 to 4 mM, yet $[Mg^{2+}]$ dependence has only been seriously investigated in troponin-based GECIs (Heim and Griesbeck, 2004; Mank et al., 2006).

We tested the effects of ionic strength, pH, and magnesium on GECIs, measuring the response of G-CaMP2 to calcium in a historical buffer (100 mM KCl, 30 mM MOPS, 10 mM K_2EGTA/CaEGTA, pH = 7.50), and mock internal solutions (135 mM KCl, 0–4 mM $MgCl_2$, 10 mM HEPES, 3 mM Na-ascorbate, 10 mM K_2EGTA/CaEGTA, pH = 7.30). The historical buffer titration gave values (calcium concentration at half-maximal fluorescence change, $K_A = 240 \pm 45$ nM; apparent Hill coefficient, $n = 3.96 \pm 0.09$; dynamic range, $F_{max}/F_{min} = 3.93 \pm 0.09$) in agreement with previous measurements (M. Kotlikoff, personal communication). However, G-CaMP2 in mock internal solution exhibited much weaker affinity, reduced cooperativity, and higher dynamic range. Increasing $[Mg^{2+}]$ decreased apparent calcium affinity and dynamic range ($K_A = 443 \pm 13$, 584 ± 30, 704 ± 37, 835 ± 71 nM; $n = 2.39 \pm 0.013$, 2.31 ± 0.024, 2.51 ± 0.024, 2.62 ± 0.038; $F_{max}/F_{min} = 6.42 \pm 0.22$, 6.25 ± 0.05, 5.81 ± 0.07, 5.50 ± 0.08 for $[Mg^{2+}] = 0, 1, 2, 4$ mM) (Fig. 2f).

Since similar binding mechanisms govern GECI signaling, the results from G-CaMP2 are likely general to other CaM-based GECIs. The accuracy of intracellular $[Ca^{2+}]$ measurement with GECIs could be improved by using affinity constants determined in the specific intracellular solution used in the patch pipette, or in a buffer that reflects cytosol if cell membrane-intact recording methods are used. Ideally, affinities should be confirmed with simultaneous *in situ* imaging of a synthetic dye (Pologruto et al., 2004). Since membrane-intact, *in situ* calibrations are inherently dynamic measurements, GECI kinetics must be considered for accurate *in situ* affinity estimates.

GECI kinetics

Neuronal calcium transients are brief. The fluorescence response of a GECI is thus highly dependent

on its kinetic properties, which are difficult to measure in a physiologically relevant context. Recently, a model of the troponin-C based GECI, TN-L15, proposed a kinetic scheme, rate constants and transfer function between calcium transients and TN-L15 response (Tay et al., 2007). Rather than precisely determine a kinetic scheme for a particular GECI, we construct a simple model to illustrate the dependence of a generic GECI's response on its kinetic rates and other intrinsic properties.

The GECI model is loosely based on G-CaMP2 recordings. All four Ca^{2+} binding events, the M13 to calmodulin binding event, chromophore activation, and all other conformational shifts leading to fluorescence, are represented in a single transition:

$$S + Ca^{2+} \underset{k_{off}}{\overset{k_{on}}{\longleftrightarrow}} S:Ca^{2+} \qquad (6)$$
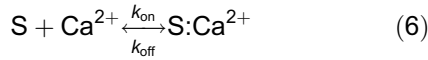
where S represents the unbound, non-fluorescent state, Ca^{2+} is free calcium and $S:Ca^{2+}$ is the bound, fluorescent state. At equilibrium, the fractional saturation state of the GECI is described by

$$\Theta = \frac{[Ca^{2+}]^n}{[Ca^{2+}]^n + K_A^n} \qquad (7)$$

$$K_A = \frac{k_{off}}{k_{on}} \qquad (8)$$

where k_{off} and k_{on} are the rates of fluorescence transition and K_A is the $[Ca^{2+}]$ at half maximal fluorescence change. The fluorescence of the GECI is related to its fractional saturation by

$$F = \Theta(F_{max} - F_{min}) + F_{min} \qquad (9)$$

or in terms of fluorescence,

$$\Theta = \left(\frac{F - F_{min}}{F_{max} - F_{min}}\right) \qquad (10)$$

For FRET and ratiometric single FP reporters, F is analogous to the ratio of the two emission wavelengths.

To quantify dynamics, we represented the change in fractional GECI saturation as the difference between second-order GECI-Ca^{2+} association and first-order dissociation:

$$\frac{d\Theta}{dt} = k_{on}(1 - \Theta)[Ca^{2+}] - k'_{off}\Theta \qquad (11)$$

To approximate the cooperativity of GECI fluorescence change, we instantaneously varied

the apparent off rate k'_{off} as a function of the fractional saturation:

$$k'_{off} = k_{off} \cdot \left(\frac{\Theta}{1 - \Theta}\right)^{\frac{1-n}{n}} \qquad (12)$$

for $\Theta < 1$.

We simulated the calcium response of a hypothetical GECI to trains of 1, 2, 3, 4, 5, 10, and 40 APs, with single-AP $\Delta[Ca^{2+}]_i = 250$ nM, $\tau = 330$ ms, $[GECI] = 10\ \mu M$, $n = 2.5$ and $F_{max}/F_{min} = 5$.

We based the kinetic parameters of the model on the best fit to 2-photon imaging of G-CaMP2 in room temperature *in utero* electroporated acute cortical slice: $K_A = 1250$ nM, $k_{on} = 8 \times 10^5$ M^{-1} s^{-1}, and $k_{off} = 1$ s^{-1} (Fig. 3a). The deviation between our *in vitro* affinity estimates and this *in situ* estimate may be due to endogenous protein interference, incomplete exchange of pipette solution and cytosol, saturation of calcium buffers (Neher, 1998) or release of intracellular calcium stores.

GECI fluorescence properties

The total dynamic range of a GECI is defined as the ratio of the signal (fluorescence intensity or acceptor-to-donor emission ratio) of the Ca^{2+}-saturated to the Ca^{2+}-free state. The effective dynamic range is defined as the ratio of the signal in saturating calcium to that at baseline calcium. The SNR, as defined in Eq. 1, scales linearly with effective dynamic range. The dynamic range of currently available GECIs has been summarized elsewhere (Garaschuk et al., 2007). The SNR ratio scales as the square root of the number of emitted photons collected, which is closely related to FP intrinsic brightness (extinction coefficient * quantum yield).

Single FP reporters conserve spectral bandwidth, allowing the stacking of additional optical readouts below and above the GFP wavelength. However, measurements must be relative to a baseline as variation in expression or excitation power directly varies fluorescence intensity. Ratiometric measurement of a two-FP GECI makes calcium measurement theoretically independent of expression level or excitation power. It also improves resistance to motion artifacts. In practice, variation in autofluoresence and cell thickness confounds single timepoint ratiometric measurements, particularly under epifluorescence illumination.

Ratiometric imaging multiplies two independent shot noise components hence is inherently noisier than single-FP imaging at the same brightness. However, FRET-based GECIs, TN-XL (Mao et al., 2008), and D3cpv (unpublished observations) expressed in cultured slice are approximately 10× brighter than G-CaMP2 in the calcium-free state. This brightness may be partially due to higher expression levels, but the intrinsic brightness of the cyan and yellow FP components are much higher than the destabilized GFP of calcium-free G-CaMP2. Due to this increased intrinsic brightness, the SNR of TN-XL and D3cpv response will be greater than G-CaMP2 for a given percent signal change.

GECI optimization

Theoretical improvements
No single GECI is optimal for all imaging experiments. The appropriate combination of intrinsic GECI parameters must be matched to the extrinsic properties of the system. These extrinsic properties include the size, shape, and the frequency of calcium transients, and baseline $[Ca^{2+}]$. Intrinsic GECI parameters include the sensor affinity, kinetics, dynamic range, brightness, expression level, and its independence from endogenous interference.

The relationship between these parameters can be illustrated by their effect on our model GECI. Varying calcium-binding affinity while holding other parameters constant reveals the tradeoffs between detection of short and long spike trains. A high GECI affinity results in a greater single-AP change in fractional saturation, facilitating detection of single (250 nM) calcium peaks. However, the sensor will saturate more easily, meaning that long spike trains may be poorly resolved. A low affinity provides a baseline F_0 (F at *resting* calcium) closer to F_{min} (F at *zero* calcium), hence a greater effective dynamic range. On the other hand, responses to small transients will be reduced. Keeping [GECI] and k_{on} constant, fluorescence response to spike trains of 1–40APs @ 83 Hz was modeled as a function of varying k_{off} ($k_{off} = 0.3$–30 s^{-1}; $K_A = 30$–3000 nM) (Fig. 3b). The K_A that maximized F_{peak}/F_0 was 180 nM for single APs ($\Delta F/F_0 = 0.14$) and 390 nM for 40AP trains ($\Delta F/F_0 = 3.23$). Affinity had a greater influence on

response of the GECI to 1AP than to 40AP (Fig. 3b, inset). The model suggests that increasing *in situ* G-CaMP2 affinity would give a significant increase in SNR. A side effect of reducing k_{off} is a resulting increase in sensor decay time, making resolution of closely spaced spikes more difficult.

The apparent GECI Ca^{2+}-binding cooperativity, n, strongly affects the optimal affinity predicted by the model (Fig. 3c). A model with large Hill coefficient ($n = 2.5$), as in G-CaMP2, gives an optimal K_A much closer to $[Ca^{2+}]_0$ than more linear models ($n = 1$, optimal $K_A = 820$ nM), comparable to *in vitro* estimates of TN-XXL (Mank and Griesbeck, 2008) and D3cpv affinity (Palmer et al., 2006) (Fig. 3c). High n also provides a higher peak response to a single AP at optimal affinity (Fig. 3c). This advantage is more pronounced with faster kinetics or greater total dynamic range (data not shown). As with high Ca^{2+}-binding affinity, high cooperativity also causes more rapid sensor saturation. It may be preferred for single-spike detection, while systems with tonic or highly modulated activity may best be measured with more linear GECIs.

The model also predicts that faster calcium-association rates will result in greater fluorescence signals. Keeping other model parameters fixed, k_{off} was varied continuously, and k_{on} was discretely increased relative to the starting value (Fig. 3d). Increasing the calcium-association rate resulted in slightly higher computed optimal affinity, and significantly larger peak fluorescence response for single transients (Fig. 3d).

Improved fluorescence properties of GECI components will also increase SNR. According to Eq. 1, the SNR of a GECI is linearly dependent on effective dynamic range (F_{max}/F_0). Since the F_0 is dependent on the total dynamic range (F_{max}/F_{min}) and the fractional saturation of the sensor at resting calcium (Eq. 9), increasing F_{max} is more effective at improving effective dynamic range when the fractional saturation at $[Ca^{2+}]_0$ is close to 0 (Fig. 3e).

Brighter GECI fluorescence yields more photons harvested during imaging, improving SNR (Eq. 1). Photobleaching is of particular concern for two-photon illumination, commonplace for *in vivo* neuronal imaging. Increased GECI photostability allows greater laser intensity, producing more photons per second. It can also increase the duration that activity can be continuously monitored. Rapid and complete chromophore maturation at physiological temperature is a prerequisite

for *in vivo* functional imaging. Incorporation of FPs with minimal sensitivity to H^+ and Cl^- ions (Tsien, 1998) or to hypothetical FRET quenchers such as ATP (Willemse et al., 2007) may also improve *in situ* brightness.

Practical improvements

Troponin C-based GECIs such as TN-L15 were designed with the goal of maximizing kinetic rates by use of a fast-binding recognition element (Heim and Griesbeck, 2004). Engineering of two EF hands of TN-L15 produced TN-XL, which shows much faster on and off rates than all other FRET-based GECIs, though is not clearly faster than G-CaMP1.6 (Mank et al., 2006). TN-XL's affinity is too weak for single AP detection. It has been enhanced by duplication of the higher affinity binding sites in the place of the lower affinity sites, at the cost of some dynamic range, to create TN-XXL (Mank and Griesbeck, 2008).

Many FRET reporters have been improved by substitution of circularly permuted FPs and linker mutagenesis, to optimize excitation and emission dipole orientation (Nagai et al., 2004; Palmer et al., 2006; Mank et al., 2006). To date, the largest observed *in vitro* FRET ratio change for a linearly fused, reversible FRET indicator is 8-fold in a prototype zinc sensor (Amy Palmer, personal communication), compared to 6.6-fold for YC2.60 and YC3.60, 5.3-fold for D3cpv, 5-fold for TN-XL, and 3.3-fold for TN-XXL (Mank and Griesbeck, 2008). Thus, a 2-fold increase in total dynamic range for FRET-based GECIs seems plausible. In the single FP instance, Case-16 shows a 16-fold $\Delta F/F_0$ *in vitro* (Souslova et al., 2007), 3-fold better than G-CaMP2. If such improvements hold *in situ*, this will result in significantly better SNR.

Brighter cyan FPs have recently been developed, such as Cerulean (Rizzo et al., 2004) or mTFP (Ai et al., 2008). Substitution of Cerulean for ECFP in cyan-to-yellow FRET sensors has improved SNR (Heim et al., 2007), though this may decrease photostability (Shaner et al., 2005). Alternative FRET pairs using GFP and tdTomato or other coral-derived FPs may have greater brightness, tissue penetration, and photostability (Shaner et al., 2005). In both cases, substitution of these proteins may necessitate sensor re-optimization, as emission dipoles and linker effects can be starkly different even with subtly different FRET pairs (Hires et al., 2008). For single-FP GECIs, the extinction coefficient and quantum yield of the

saturated state of G-CaMP2 (Tallini et al., 2006) could potentially be increased to the level of EGFP.

GECIs ideally should not respond to non-target stimuli such as other divalent cations, which may not correlate with neural activity. Cameleon emission spectra are not directly changed by $[Mg^{2+}]$ (Miyawaki et al., 1997), but the effect of Mg^{2+} on cameleon-Ca^{2+} titration curves has not been published. Mg^{2+} may compete with Ca^{2+} at certain binding sites without inducing a significant conformational change in cameleons. Calcium titration curves of the troponin C-based GECI TN-L15 showed strong Mg^{2+}-sensitivity (Heim and Griesbeck, 2004). Rational engineering of two EF hands within troponin-C produced TN-XL (Mank et al., 2006), with greatly reduced Mg^{2+}-sensitivity. Similarly, GECIs should not interact with endogenous calcium-binding proteins. Computational "bump-hole" redesign of the calmodulin-M13pep interface within the context of an ECFP-cpVenus FRET sensor produced the D2cpv, D3cpv, and D4cpv class of cameleons (Palmer et al., 2006). These redesigned GECIs performed much better than YC3.3 in membrane-targeted constructs imaged in dissociated hippocampal neurons (Palmer et al., 2006). However, the computational redesign was performed on a significantly different calmodulin-binding peptide than previous cameleons preventing direct comparison.

GECI testing standardization

The performance of various GECIs has been determined in a wide variety of systems. However, comparing their performance between different *in vitro*, *in situ*, and various species of *in vivo* preps is difficult, as each system has substantially different extrinsic parameters. Some diversity in test systems is warranted; performance in mice will depend on different parameters than performance in flies or worms. However, consolidation and standardization of test systems would benefit GECI developers and end-users.

An ideal testing standard should encompass as many aspects of the final measurement system as possible. This standard must be sensitive to both affinity and kinetics. Predicting GECI responses to dynamic calcium transients from equilibrium binding experiments alone is futile. Correspondingly, testing should be done at physiological temperature. The

calcium transient must be reliably produced and accessible by independent measurement. It should approximate the time course of the signal that ultimately will be measured. If produced by a natural stimulus, the mean and variance of the number of APs it drives and the contribution of synaptic input must be known. To prevent GECI washout and retain effects of expression and interference, the intracellular milieu should be unperturbed. Practically, the method should retain sufficient throughput to assess newly obtained GECIs with minimal delay. It should also be cost-effective and accessible to a large number of imaging and physiology labs.

Most non-neuronal cell types lack sufficient calcium extrusion machinery to rapidly ($\ll$1 s) clear intracellular calcium, making a test in those cells insensitive to sensor kinetics. In dissociated neuronal cultures, the network connectivity and extracellular milieu is dramatically disrupted, which may change the expression patterns of calcium channels and increase response heterogeneity. Cultured slices give anomalously large responses compared to acute slices (Mao et al., 2008). Although cultured neurons can provide a high throughput for screening large numbers of potential sensors, they are imperfect for careful comparison of a small number of high quality sensors.

Recent experiments have established a standard that captures many aspects of *in vivo* functional imaging of mice. This standard is 2-photon imaging of GECI responses to back-propagating APs in acute brain slice. The APs are driven by intermittent 2 ms depolarizing pulses (Pologruto et al., 2004; Mao et al., 2008), or by continuous current injection (Heim et al., 2007) from a patch pipette. Intermittent stimulation offers greater control over spike timing and frequency. Continuous depolarization may cause significant calcium flux during the inter-spike interval, which could overestimate the GECI response to naturally occurring spike trains. With both techniques, spontaneous activity is silenced with glutamate receptor blockers, so the potential confound of synaptic input is avoided. The calcium transients associated with back-propagating APs have been well characterized, and slice imaging is amenable to $\Delta[Ca^{2+}]_i$ confirmation with a synthetic dye. Slices can be recorded at room temperature or physiological temperature. Since the GECI is expressed from a prenatal period, developmental and interference effects will be captured. Recording can be done with high-resistance electrodes or *via* perforated

patch to reduce or prevent dialysis of intracellular components.

This technique has a moderate throughput. In conjunction with *in utero* electroporation, acute slice imaging allows thorough characterization of around two GECIs per person, per week. The delay between plasmid construction and response characterization is 3 weeks. Excluding the fixed costs of an imaging and physiology rig, testing of novel GECIs via *in utero* electroporation is inexpensive compared to virus or transgenic animal production.

There are a few parameters that this method does not fully capture. *In utero* electroporation does not drive very high expression levels. In neurons that highly expressed G-CaMP2, sensor invaded the nucleus and performance was poor (data not shown). GECIs with reduced interference, such as TN-XXL or D3cpv, might show higher relative performance when driven by powerful promoters introduced by virus. *In vivo* imaging has more challenging SNR requirements due to greater imaging depth and motion artifacts. However, mice from the same litter of *in utero* electroporated animals can be simultaneously tested in brain slice and *in vivo* preps. This can easily confirm the predictive power of this testing method.

Combined optical stimulation and recording

Genetically encoded optical tools for the control of membrane potential have improved dramatically over the past several years. However, the action spectrum of the neuronal activating channelrhodopsin-2 (ChR2) (Zhang et al., 2006) and neuronal silencing halorhodopsin (NpHR) (Han and Boyden, 2007; Zhang et al., 2007) overlap with the excitation or emission spectra of currently available GECIs. Far red-shifted variants of ChR2 may permit continuous monitoring of calcium responses during stimulation (Zhang et al., 2008). However, these variants are still in developmental stages and have not been well characterized in *in vivo* systems. Gated illumination protocols should allow combined neuronal stimulation with GECI monitoring using standard ChR2 and any major class of GECI.

ChR2 requires a brief pulse (1–10 ms) of spatially broad, bright illumination to induce AP firing. At light intensities used for calcium imaging,

two-photon laser scanning illumination of ChR2 does not cause membrane depolarization (Zhang and Oertner, 2007). Calcium transients persist for hundreds of milliseconds and are typically acquired at 4–8 Hz *in vivo*. Two-photon laser scanning can be used to excite the GECI, widefield blue light used to stimulate ChR2, and the GECI emission channels can be gated during the ChR2 stimulation pulses. Precise gating during a 1AP stimulation will cause a loss of GECI signal from only a small fraction of the field of view for a single timepoint.

Since neuronal silencing via NpHR requires continuous illumination, gating during optical silencing will have a greater impact on GECI signal collection. However, NpHR's action spectrum extends to wavelengths longer than 600 nm (Han and Boyden, 2007). Simultaneous two-photon imaging of a GECI during long wavelength excitation of NpHR should be possible with appropriate selection of interference filters. This could also be combined with ChR2 gating for bi-directional optical neuronal control and recording.

In vivo imaging

What level of improvement in SNR of currently available GECIs is needed to reliably detect single APs *in vivo*? Currently, the response to single APs of G-CaMP2 or TN-XL is buried in the noise floor of acute slice (Figs. 2a, b, and 3a) (Mao et al., 2008; Heim et al., 2007). In cultured slice at room temperature, a burst of four APs at 83 Hz was required for $>90\%$ reliable detection of G-CaMP2 signal, while 10 AP were required at 35°C (Mao et al., 2008). Both burst conditions had an average peak $\Delta F/F_0$ of approximately 60%, with the smallest detectable response of approximately 30% $\Delta F/F_0$ (Mao et al., 2008). Brighter GECIs, such as D3cpv and TnC-based sensors should have significantly lower thresholds, due to reduced noise. In acute cortical slice from transgenic CerTN-L15 mice, continuous current injections that caused a two AP burst gave $\Delta R/R_0$ of 13%. These were detectable, though reliability statistics were not published (Heim et al., 2007).

The noise level *in vivo* is generally worse than in brain slice. It is dependent on specifics of the imaging setup, on GECI brightness, expression level, and cell depth, so determining the exact amount of improvement needed for reliable single

AP detection is impossible. As a rough guide, glutamate-induced dendritic transients of CerTN-L15 *in vivo* had a $\Delta R/R_0$ of 49% and peak-to-peak noise of approximately 15% in single trials (Heim et al., 2007). The effects of various GECI improvements on reaching *in vivo* detection thresholds are predictable. Kinetic rates of most biological processes increase between room temperature and 37°C. Peak G-CaMP2 responses recorded at 35°C in acute slice are reported to be reduced by about 50% in amplitude and have ~3-fold faster decay time than at 22°C (Mao et al., 2008). The faster decay is likely due to a combination of an increase in speed of the underlying transient, due to faster calcium extrusion, and an increase in G-CaMP2 kinetics. The reduction in peak response suggests that the temperature dependence of Ca^{2+}-binding to G-CaMP2 is less than that of the calcium extrusion rate. Using calcium transients from dendritic measurements made at physiological temperatures ($\tau = 70$ ms) (Markram et al., 1995) reduces the 1AP response of an optimal affinity GECI from 0.14 to 0.04 $\Delta F/F_0$, assuming no corresponding increase in GECI kinetics (Fig. 3f). A plausible future improvement of F_{max}/F_{min} to 15-fold increases the response to 0.12 $\Delta F/F_0$. As GECI kinetic rates increase, either through the temperature dependence or engineering, the 1AP response reaches levels that should allow reliable *in vivo* detection (Fig. 3f), with the exact threshold determined by brightness and expression level. Although there is no single "magic bullet" to make GECIs reach performance levels equivalent to synthetic indicators, concerted optimization of the numerous factors explored here provides a plausible route to consistent single AP detection.

Conclusion

GECIs have come a long way in the decade since their creation; nearly every relevant biophysical parameter has been improved relative to the first generation. Increases in baseline brightness and relative signal change have contributed to enhanced SNR ratio. Rational engineering of GECI components has produced variants with decreased interaction with endogenous proteins, facilitating long-term imaging experiments at higher expression levels with fewer non-target effects. Concomitant with sensor improvements, systematic

optimization of data collection, filtering, and analysis techniques has improved spike detection (Yaksi and Friedrich, 2006). Several classes of GECIs have performed well for neural imaging, encompassing single-FP and FRET sensors, and sensors based on calmodulin and troponin-C calcium-binding domains. Published GECIs are adequate for detecting high frequency bursts of neuronal activity, making them appropriate for activity localization in mouse myotubes (Nakai et al., 2001), mouse cerebellum (Diez-Garcia et al., 2005), or in invertebrate systems (Kerr et al., 2000; Higashijima et al., 2003; Wang et al., 2003; Chronis et al., 2007; Clark et al., 2007). However, reliable *in vivo* single-AP detection is not yet feasible with the current generation of techniques. For the moment, projects seeking to image sparsely encoded information will best be served by bulk loading of small molecule dyes, despite the limitations of an acute time course, difficult loading, poor cellular specificity, and neuropil signal contamination (Kerr and Denk, 2008).

Future protein engineering efforts will primarily focus on improving GECI SNR. Incremental increases to existing GECIs appear sufficient to reach single-AP detection, but novel scaffolds may be found with even greater performance. Structural analysis of GECIs *via* X-ray crystallography or NMR may help elucidate their Ca^{2+}-dependent reporting mechanism, particularly if structural information can be obtained in both the Ca^{2+}-free and Ca^{2+}-bound states. This could aid in the optimization of existing sensors and the engineering of new ones. It must also be ensured that GECIs are amenable to long-term expression and imaging in animals. This may involve iterative negative design against endogenous interactions and use of inducible, reversible promoters (Hasan et al., 2004).

GECIs must be prototyped in a way that will accurately predict their performance in functional imaging studies. Broad use of a standard assay in a well-defined biological system will ensure that the best GECIs are prioritized for further testing and eventual construction of transgenic lines. Systematic optimization of individual sensor components, allosteric response mechanisms, and overall performance in a realistic assay, will lead to dramatic improvements in many GECI formats in the near term. The goal of imaging sparse firing *in vivo* with GECIs requires much work, but the prospect of long-term, high resolution, non-invasive *in vivo* functional imaging in defined cell populations guarantees that it will be worth the effort.

Methods

In vitro characterization—G-CaMP2 was expressed in *Escherichia coli* BL21 (DE3) using a pRSETB plasmid, and purified via a 6His-NiNTA system. Following buffer exchange to 100 mM NaCl, 20 mM Tris, pH 7.5, protein was diluted ~200-fold to 1 μM [G-CaMP2] in a historical buffer of 100 mM KCl, 30 mM MOPS, pH 7.5, or mock internal solution of 135 mM KCl, 0–4 mM $MgCl_2$, 10 mM HEPES, 3 mM Na-ascorbate, pH 7.3. These solutions were supplemented with a 10 mM blend of K_2H_2EGTA and CaEGTA from the concentrated Calcium Calibration Kit (Invitrogen) in various ratios to control free calcium concentration. The pH probe was calibrated and solution acidity adjusted with small volumes of KOH and HCl while submerged in a water bath maintained at 28°C. Four sets of titration points for each condition were measured three times on a Safire[2] fluorescence plate reader (Tecan) with excitation at 470 nm and emission at 510 nm, bandwidth 15 nm, then averaged.

To estimate intracellular [G-CaMP2], purified G-CaMP2 in pipette internal solution supplemented with 1 mM K_2EGTA was drawn into thin glass capillaries (ID = 0.02 mm, Vitrocom #RT5002) at 0.1, 1, and 10 μM concentrations. Their fluorescence intensity was measured under 2-photon excitation parameters identical (910 nm) to slice imaging. These intensities were compared to those of the recorded G-CaMP2 cells. Expression was estimated by assuming fluorescence per molecule of G-CaMP2 was identical between purified and intracellular G-CaMP2.

Slice preparation and recording
In utero electroporation and acute slice preparation was done as previously described (Mao et al., 2008). After 1 h pre-incubation, slices were transferred to an immersion-type recording chamber and perfused with ACSF comprising (in mM) 127 NaCl, 2.5 KCl, 1.25 NaH_2PO_4, 25 D-glucose, 25 $NaHCO_3$, 4 $CaCl_2$, and 4 $MgCl_2$ saturated with 95% O_2/5% CO_2 and with 25 μM (R)-CPP (Tocris) and 25 μM NBQX (Sigma) to block glutamate receptors. Recordings were performed at room temperature (22°C). Neurons were visualized under infrared

differential interference optics and patched with borosilicate pipettes (resistance 4–6 MΩ). The intracellular solution contained (in mM) 128 K-gluconate, 10 HEPES, 10 Na_2-phosphocreatine, 4 Na_2-ATP, 0.4 Na-GTP, 4 $MgCl_2$, 0.4 Na_2-GTP, and 3 Na-ascorbate (pH 7.27; 287 mOsm). Cells were recorded at a depth of 50–95 μm in the brain slice.

Imaging was performed as previously described (Mao et al., 2008). Neurons were imaged in line-scan mode (500 Hz) across a location 20–40 μm from the base of the apical dendrite using 2-photon excitation from a Ti:sapphire laser (Mira, Coherent, Santa Clara, CA, USA) tuned to 910 nm. Fluorescence was collected in two channels in both epi- and trans-fluorescence mode using four photomultiplier tubes (Hamamatsu, Hamamatsu City, Japan), then separated into green and red channels with 565 nm dichroics and BG22 (green) and HQ620/90 (red) emission filters. PMT dark noise was subtracted from all traces. Crosstalk between emission channels was negligible. Peak fluorescence was determined by averaging 30 ms of the raw fluorescence time series about the peak of the trace linearly filtered at 30 Hz. Data were acquired and analyzed with custom Matlab software (Mathworks).

GECI modeling
Simulations of calcium transients and GECI response were performed in Matlab. Euler's method was used for time discretization with a time step of 20 μs. Matlab notebooks used for modeling calcium transients and GECI responses are available on the *Brain Cell Biology* website.

Acknowledgments

Open Access

References

Ai, H. W., Olenych, S. G., Wong, P., Davidson, M. W., and Campbell, R. E. (2008). Hue-shifted monomeric variants of Clavularia cyan fluorescent protein: identification of the molecular determinants of color and applications in fluorescence imaging. BMC Biol. *6*, 13.

Baird, G. S., Zacharias, D. A., and Tsien, R. Y. (1999). Circular permutation and receptor insertion within green fluorescent proteins. Proc. Natl Acad. Sci. USA *96*, 11241–11246.

Burgoyne, R. D. (2007). Neuronal calcium sensor proteins: generating diversity in neuronal Ca2+ signalling. Nat. Rev. Neurosci. *8*, 182–193.

Chronis, N., Zimmer, M., and Bargmann, C. I. (2007). Microfluidics for *in vivo* imaging of neuronal and behavioral activity in *Caenorhabditis elegans*. Nat. Method. *4*, 727–731.

Clark, D. A., Gabel, C. V., Gabel, H., and Samuel, A. D. (2007). Temporal activity patterns in thermosensory neurons of freely moving *Caenorhabditis elegans* encode spatial thermal gradients. J. Neurosci. *27*, 6083–6090.

Denk, W., Yuste, R., Svoboda, K., and Tank, D. W. (1996). Imaging calcium dynamics in dendritic spines. Curr. Opin. Neurobiol. *6*, 372–378.

Di Virgilio, F., Steinberg, T. H., Swanson, J. A., and Silverstein, S. C. (1988). Fura-2 secretion and sequestration in macrophages. A blocker of organic anion transport reveals that these processes occur via a membrane transport system for organic anions. J. Immunol. *140*, 915–920.

Diez-Garcia, J., Matsushita, S., Mutoh, H., Nakai, J., Ohkura, M., Yokoyama, J. et al. (2005). Activation of cerebellar parallel fibers monitored in transgenic mice expressing a fluorescent Ca^{2+} indicator protein. Eur. J. Neurosci. *22*, 627–635.

Ferkey, D. M., Hyde, R., Haspel, G., Dionne, H. M., Hess, H. A., Suzuki, H. et al. (2007). *C. elegans* G protein regulator RGS-3 controls sensitivity to sensory stimuli. Neuron *53*, 39–52.

Fiala, A., Spall, T., Diegelmann, S., Eisermann, B., Sachse, S., Devaud, J. M. et al. (2002). Genetically expressed cameleon in Drosophila melanogaster is used to visualize olfactory information in projection neurons. Curr. Biol. *12*, 1877–1884.

Furler, S., Paterna, J. C., Weibel, M., and Bueler, H. (2001). Recombinant AAV vectors containing the foot and mouth disease virus 2A sequence confer efficient bicistronic gene expression in cultured cells and rat substantia nigra neurons. Gene Ther. *8*, 864–873.

Garaschuk, O., Griesbeck, O., and Konnerth, A. (2007). Troponin C-based biosensors: a new family of genetically encoded indicators for *in vivo* calcium imaging in the nervous system. Cell Calcium *42*, 351–361.

Grynkiewicz, G., Poenie, M., and Tsien, R. Y. (1985). A new generation of Ca^{2+} indicators with greatly improved fluorescence properties. J. Biol. Chem. *260*, 3440–3450.

Han, X. and Boyden, E. S. (2007). Multiple-color optical activation, silencing, and desynchronization of neural activity, with single-spike temporal resolution. PLoS ONE *2*, e299.

Hasan, M. T., Friedrich, R. W., Euler, T., Larkum, M. E., Giese, G., Both, M. et al. (2004). Functional fluorescent Ca^{2+} indicator proteins in transgenic mice under TET control. PLoS Biol. *2*, e163.

Haugland, R. P., Spence, M. T. Z., Johnson, I. D., and Basey, A. (2005). The Handbook: A Guide to Fluorescent Probes and Labeling Technologies, 10th ed., Molecular Probes, Eugene, OR.

Heim, N. and Griesbeck, O. (2004). Genetically encoded indicators of cellular calcium dynamics based on troponin C and green fluorescent protein. J. Biol. Chem. *279*, 14280–14286.

Heim, N., Garaschuk, O., Friedrich, M. W., Mank, M., Milos, R. I., Kovalchuk, Y. et al. (2007). Improved calcium imaging in transgenic mice expressing a troponin C-based biosensor. Nat. Method *4*, 127–129.

Helmchen, F., Imoto, K., and Sakmann, B. (1996). Ca^{2+} buffering and action potential-evoked Ca^{2+} signaling in dendrites of pyramidal neurons. Biophys. J. *70*, 1069–1081.

Higashijima, S., Masino, M. A., Mandel, G., and Fetcho, J. R. (2003). Imaging neuronal activity during zebrafish behavior with a genetically encoded calcium indicator. J. Neurophysiol. *90*, 3986–3997.

Hille, B. (1992). Ionic Channels of Excitable Membranes, 2nd. ed., Sinauer Associates, Sunderland, MA.

Hires, S. A., Zhu, Y., and Tsien, R. Y. (2008). Optical measurement of synaptic glutamate spillover and reuptake by linker optimized glutamate-sensitive fluorescent reporters. Proc. Natl. Acad. Sci. USA *105*, 4411–4416.

Jaffe, D. B., Johnston, D., Lasser-Ross, N., Lisman, J. E., Miyakawa, H., and Ross, W. N. (1992). The spread of Na+ spikes determines the pattern of dendritic Ca^{2+} entry into hippocampal neurons. Nature *357*, 244–246.

Jayaraman, V., and Laurent, G. (2007). Evaluating a genetically encoded optical sensor of neural activity using electrophysiology in intact adult fruit flies. Front. Neural Circ. *1*. doi:10.3389/neuro.04.003.2007.

Johnson, F. H. and Shimomura, O. (1972). Preparation and use of aequorin for rapid microdetermination of Ca^{2+} in biological systems. Nat. New. Biol. *237*, 287–288.

Kerr, J. N. and Denk, W. (2008). Imaging *in vivo*: watching the brain in action. Nat. Rev. Neurosci. *9*, 195–205.

Kerr, R., Lev-Ram, V., Baird, G., Vincent, P., Tsien, R. Y., and Schafer, W. R. (2000). Optical imaging of calcium transients in neurons and pharyngeal muscle of *C. elegans*. Neuron *26*, 583–594.

Kerr, R. A. and Schafer, W. R. (2006). Intracellular Ca^{2+} imaging in *C. elegans*. Method. Mol. Biol. *351*, 253–264.

Kindt, K. S., Quast, K. B., Giles, A. C., De, S., Hendrey, D., Nicastro, I. et al. (2007). Dopamine mediates context-dependent modulation of sensory plasticity in *C. elegans*. Neuron *55*, 662–676.

Kotlikoff, M. I. (2007). Genetically encoded Ca^{2+} indicators: using genetics and molecular design to understand complex physiology. J. Physiol. *578*, 55–67.

Linse, S., Helmersson, A., and Forsen, S. (1991). Calcium binding to calmodulin and its globular domains. J. Biol. Chem. *266*, 8050–8054.

Llinas, R., Sugimori, M., and Simon, S. M. (1982). Transmission by presynaptic spike-like depolarization in the squid giant synapse. Proc. Natl. Acad. Sci. USA *79*, 2415–2419.

Mank, M., and Griesbeck, O. (2008). Genetically encoded calcium indicators. Chem. Rev. *108*, 1550–1564.

Mank, M., Reiff, D. F., Heim, N., Friedrich, M. W., Borst, A., and Griesbeck, O. (2006). A FRET-based calcium biosensor with fast signal kinetics and high fluorescence change. Biophys. J. *90*, 1790–1796.

Mao, T., O'Connor, D. H., Scheuss, V., Nakai, J., and Svoboda, K. (2008). Characterization and subcellular targeting of GCaMP-type genetically-encoded calcium indicators. PLoS ONE *3*, e1796.

Markram, H. and Sakmann, B. (1994). Calcium transients in dendrites of neocortical neurons evoked by single subthreshold excitatory post-synaptic potentials via low-voltage-activated calcium channels. Proc. Natl. Acad. Sci. USA *91*, 5207–5211.

Markram, H., Helm, P. J., and Sakmann, B. (1995). Dendritic calcium transients evoked by single back-propagating action potentials in rat neo-cortical pyramidal neurons. J. Physiol. *485*, 1–20.

Minta, A., Kao, J. P., and Tsien, R. Y. (1989). Fluorescent indicators for cytosolic calcium based on rhodamine and fluorescein chromophores. J. Biol. Chem. *264*, 8171–8178.

Miyawaki, A. and Tsien, R. Y. (2000). Monitoring protein conformations and interactions by fluorescence resonance energy transfer between mutants of green fluorescent protein. Method. Enzymol. *327*, 472–500.

Miyawaki, A., Llopis, J., Heim, R., McCaffery, J. M., Adams, J. A., Ikura, M. et al. (1997). Fluorescent indicators for Ca^{2+} based on green fluorescent proteins and calmodulin. Nature *388*, 882–887.

Miyawaki, A., Griesbeck, O., Heim, R., and Tsien, R. Y. (1999). Dynamic and quantitative Ca^{2+} measurements using improved cameleons. Proc. Natl. Acad. Sci. USA *96*, 2135–2140.

Muller, W. and Connor, J. A. (1991). Dendritic spines as individual neuronal compartments for synaptic Ca^{2+} responses. Nature *354*, 73–76.

Nagai, T., Sawano, A., Park, E. S., and Miyawaki, A. (2001). Circularly permuted green fluorescent proteins engineered to sense Ca^{2+}. Proc. Natl. Acad. Sci. USA *98*, 3197–3202.

Nagai, T., Yamada, S., Tominaga, T., Ichikawa, M., and Miyawaki, A. (2004). Expanded dynamic range of fluorescent indicators for Ca^{2+} by circularly permuted yellow fluorescent proteins. Proc. Natl. Acad. Sci. USA *101*, 10554–10559.

Nakai, J., Ohkura, M., and Imoto, K. (2001). A high signal-to-noise Ca(2+) probe composed of a single green fluorescent protein. Nat. Biotechnol. *19*, 137–141.

Neher, E. (1995). The use of fura-2 for estimating Ca buffers and Ca fluxes. Neuropharmacology *34*, 1423–1442.

Neher, E. (1998). Usefulness and limitations of linear approximations to the understanding of Ca^{++} signals. Cell Calcium *24*, 345–357.

Ogawa, Y. and Tanokura, M. (1984). Calcium binding to calmodulin: effects of ionic strength, Mg2+, pH and temperature. J. Biochem. *95*, 19–28.

Ohkura, M., Matsuzaki, M., Kasai, H., Imoto, K., and Nakai, J. (2005). Genetically encoded bright Ca^{2+} probe applicable for dynamic Ca^{2+} imaging of dendritic spines. Anal. Chem. *77*, 5861–5869.

Palmer, A. E. and Tsien, R. Y. (2006). Measuring calcium signaling using genetically targetable fluorescent indicators. Nat. Protoc. *1*, 1057–1065.

Palmer, A. E., Giacomello, M., Kortemme, T., Hires, S. A., Lev-Ram, V., Baker, D. et al. (2006). Ca^{2+} indicators based on computationally redesigned calmodulin-peptide pairs. Chem. Biol. *13*, 521–530.

Pelletier, J. and Sonenberg, N. (1988). Internal initiation of translation of eukaryotic mRNA directed by a sequence derived from poliovirus RNA. Nature *334*, 320–325.

Pologruto, T. A., Yasuda, R., and Svoboda, K. (2004). Monitoring neural activity and $[Ca^{2+}]$ with genetically encoded Ca^{2+} indicators. J. Neurosci. *24*, 9572–9579.

Reiff, D. F., Ihring, A., Guerrero, G., Isacoff, E. Y., Joesch, M., Nakai, J. et al. (2005). *In vivo* performance of genetically encoded indicators of neural activity in flies. J. Neurosci. *25*, 4766–4778.

Rink, T. J., Tsien, R. Y., and Warner, A. E. (1980). Free calcium in Xenopus embryos measured with ion-selective microelectrodes. Nature *283*, 658–660.

Rizzo, M. A., Springer, G. H., Granada, B., and Piston, D. W. (2004). An improved cyan fluorescent protein variant useful for FRET. Nat. Biotechnol. *22*, 445–449.

Schiller, J., Helmchen, F., and Sakmann, B. (1995). Spatial profile of dendritic calcium transients

evoked by action potentials in rat neocortical pyramidal neurones. J. Physiol. *487*, 583–600.

Shaner, N. C., Steinbach, P. A., and Tsien, R. Y. (2005). A guide to choosing fluorescent proteins. Nat. Method. *2*, 905–909.

Shimozono, S. and Miyawaki, A. (2008). Engineering FRET constructs using CFP and YFP. Method. Cell Biol. *85*, 381–393.

Souslova, E. A., Belousov, V. V., Lock, J. G., Stromblad, S., Kasparov, S., Bolshakov, A. P. et al. (2007). Single fluorescent protein-based Ca^{2+} sensors with increased dynamic range. BMC Biotechnol. *7*, 37.

Suzuki, H., Kerr, R., Bianchi, L., Frokjaer-Jensen, C., Slone, D., Xue, J. et al. (2003). *In vivo* imaging of *C. elegans* mechanosensory neurons demonstrates a specific role for the MEC-4 channel in the process of gentle touch sensation. Neuron *39*, 1005–1017.

Tallini, Y. N., Ohkura, M., Choi, B. R., Ji, G., Imoto, K., Doran, R. et al. (2006). Imaging cellular signals in the heart *in vivo*: cardiac expression of the high-signal Ca^{2+} indicator GCaMP2. Proc. Natl. Acad. Sci. USA *103*, 4753–4758.

Tay, L. H., Griesbeck, O., and Yue, D. T. (2007). Live-cell transforms between Ca^{2+} transients and FRET responses for a troponin-C-based Ca^{2+} sensor. Biophys. J. *93*, 4031–4040.

Tour, O., Adams, S. R., Kerr, R. A., Meijer, R. M., Sejnowski, T. J., Tsien, R. W. et al. (2007). Calcium Green FlAsH as a genetically targeted small-molecule calcium indicator. Nat. Chem. Biol. *3*, 423–431.

Truong, K., Sawano, A., Miyawaki, A., and Ikura, M. (2007). Calcium indicators based on calmodulin-fluorescent protein fusions. Methods Mol. Biol. *352*, 71–82.

Tsai, P. S., Friedman, B., Ifarraguerri, A. I., Thompson, B. D., Lev-Ram, V., Schaffer, C. B. et al. (2003). All-optical histology using ultrashort laser pulses. Neuron *39*, 27–41.

Tsien, R. Y. (1980). New calcium indicators and buffers with high selectivity against magnesium and protons: design, synthesis, and properties of prototype structures. Biochemistry *19*, 2396–2404.

Tsien, R. Y. (1998). The green fluorescent protein. Annu. Rev. Biochem. *67*, 509–544.

Tsien, R. Y. (1999). Monitoring cell calcium. In: Carafoli, E., Klee, C. B. (eds.) Calcium as a cellular regulator, Oxford University Press, USA, pp. 28–54.

Tsien, R. Y. and Rink, T. J. (1983). Measurement of cytoplasmic free Ca^{2+}. In: Barker, J., McKelvey, J. F. (eds.) Current Methods of Cellular Neurobiology, 3rd. ed., Wiley, New York.

Wang, J. W., Wong, A. M., Flores, J., Vosshall, L. B., and Axel, R. (2003). Two-photon calcium imaging reveals an odor-evoked map of activity in the fly brain. Cell *112*, 271–282.

Willemse, M., Janssen, E., de Lange, F., Wieringa, B., and Fransen, J. (2007). ATP and FRET—a cautionary note. Nat. Biotechnol. *25*, 170–172.

Yaksi, E. and Friedrich, R. W. (2006). Reconstruction of firing rate changes across neuronal populations by temporally deconvolved Ca^{2+} imaging. Nat. Method. *3*, 377–383.

Yang, Y., Costa, A., Leonhardt, N., Siegel, R. S., and Schroeder, J. I. (2008). Isolation of a strong Arabidopsis guard cell promoter and its potential as a research tool. Plant Method. *4*, 6.

Yasuda, R., Nimchinsky, E. A., Scheuss, V., Pologruto, T. A., Oertner, T. G., Sabatini, B. L., et al. (2004). Imaging calcium concentration dynamics in small neuronal compartments. Sci. STKE *2004*, l5.

Yuste, R. and Denk, W. (1995). Dendritic spines as basic functional units of neuronal integration. Nature *375*, 682–684.

Yuste, R., Majewska, A., Cash, S. S., and Denk, W. (1999). Mechanisms of calcium influx into hippocampal spines: heterogeneity among spines, coincidence detection by NMDA receptors, and optical quantal analysis. J. Neurosci. *19*, 1976–1987.

Zhang, Y. P. and Oertner, T. G. (2007). Optical induction of synaptic plasticity using a light-sensitive channel. Nat. Method. *4*, 139–141.

Zhang, F., Wang, L. P., Boyden, E. S., and Deisseroth, K. (2006). Channelrhodopsin-2 and optical control of excitable cells. Nat. Method. *3*, 785–792.

Zhang, F., Wang, L. P., Brauner, M., Liewald, J. F., Kay, K., Watzke, N. et al. (2007). Multimodal fast optical interrogation of neural circuitry. Nature *446*, 633–639.

Zhang, F., Prigge, M., Beyriere, F., Tsunoda, S. P., Mattis, J., Yizhar, O. et al. (2008). Red-shifted optogenetic excitation: a tool for fast neural control derived from Volvox carteri. Nat. Neurosci. *11*, 631–633.